

Residual Mechanical Properties and Explosive Spalling Behavior of Ultra-High-Strength Concrete Exposed to High Temperature

Gaifei Peng and Juan Yang*

(Faculty of Civil Engineering, Beijing Jiaotong University, Beijing 100044, China)

Abstract: In order to explore the characteristics of ultra-high-strength concrete exposed to high temperature, residual mechanical properties and explosive spalling behavior of ultra-high-strength concrete (UHSC) and high strength concrete (HSC) exposed to high temperatures ranging from 20 °C to 800 °C were determined. The microstructure of the specimens after exposure to elevated temperature was analyzed by means of scanning electron microscope (SEM) and mercury intrusion porosimetry (MIP). The residual compressive strengths of UHSC and HSC were first increased and then decreased as temperature increased. After exposure to 800 °C, the compressive strengths of UHSC and HSC were 24.2 % and 22.3 % of their original strengths at 20 °C, respectively. The residual splitting tensile strengths of both UHSC and HSC were consistently decreased with the temperature increasing and were approximately 20% of their original strengths after 800 °C. However, the residual fracture energies of both concretes tended to ascend even at 600 °C. The explosive spalling of UHSC was more serious than that of HSC. Moisture content of the specimens governs the explosive spalling of both concretes with a positive correlations, and it is more pronounced in UHSC. These results suggest that UHSC suffers a substantial loss in load-bearing capacity and is highly prone to explosive spalling due to high temperature. The changes in compressive strength are due to the changes in the density and the pore structure of concrete. The probability and severity of explosive spalling of UHSC are much higher than those of HSC due to the higher pore volume in HSC.

Keywords: ultra-high-strength concrete; high strength concrete; residual mechanical properties; explosive spalling

CLC number: TU528.3

Document code: A

Article ID: 1005-9113(2017)04-0062-09

1 Introduction

Characterized by ultra-high compressive strength and ultra-high durability, ultra-high-strength concrete (UHSC) that incorporated coarse aggregates has been increasingly used in engineering structures, such as ultra-high rise buildings in Japan^[1], military shielding panels in Germany^[2], and the National Great Theater^[3], the International Finance Center^[4], and the Huangchao Wanxin building^[5] in China. However, UHSC is highly prone to explosive spalling when exposed to elevated temperature and/or fire due to its high compactness and low permeability. Thus, comprehensive characterization of UHSC's fire damage and explosive spalling behavior in UHSC exposed to elevated temperature is of great concern.

The influences of high temperature or fire on the properties of UHSC have been investigated. Study on the influences of coarse aggregates on explosive spalling

behavior of UHSC indicated that the explosive spalling was more severe when raw materials contain andesite and limestone, but a little or no explosive spalling occurred when quartzite and hardened sandstone were added^[6]. Besides, moisture content is the major factor that induces explosive spalling in UHSC, especially in the concrete surface layer^[7]. D. Hosser^[8] reported the beneficial effect of basalt on mitigating the explosive spalling of UHSC. An experimental study has reported the serious explosive spalling of plain UHSC, but polypropylene fiber (PP fiber) inhibited the degree of spalling^[9]. Another study confirmed that PP fiber with the dosage of 0.20% volume may prevent spalling, whereas spalling occurred at a dosage of 0.30%^[10]. Other studies have presented different findings regarding the effects of PP fiber on the explosive spalling of UHSC. PP fiber efficiently prevents explosive spalling of UHSC with compressive strength of below 150 MPa, while the beneficial effect of PP fiber tends to disappear when it is above 180 MPa. However, hybrid fiber

Received 2016-04-21.

Sponsored by the National Natural Science Foundation of China (Grant No.51278048) and the Fundamental Research Funds for the Central Universities of China (Grant No.C11JB00720).

* Corresponding author. E-mail: wechico@163.com.

(0.5% steel fiber and 0.33% PP fiber) can prevent spalling regardless of the compressive strength of UHSC^[11]. However, a comprehensive study on the residual mechanical properties and explosive spalling behavior of both UHSC and HSC has been rarely reported.

A risk of explosive spalling exists in UHSC, and this can endanger the entire structure using UHSC. Thus, fire resistance of UHSC needs to be further studied. To explore the fire resistance of UHSC and its difference from that of HSC, residual mechanical properties and explosive spalling behavior of UHSC and HSC exposed to high temperature were measured in this study. To explore the correlation between the changes in microstructure and the properties at macro-scale, including compressive strength and explosive spalling behavior, microstructure of concrete was analyzed by means of scanning electron microscope (SEM) and mercury intrusion porosimetry (MIP).

2 Experimental Details

2.1 Materials

Coarse aggregates in this study were basalts with two particle size ranges (5–10 mm and 10–16 mm) in a mass proportion of 3 : 7, and its physical properties

are listed in Table 1. Artificial sand was used as fine aggregate, and its physical properties are shown in Table 2. Portland cement (52.5R) and mineral admixtures including silica fume (SF), fly ash (FA), and ground-granulated blast furnace slag (GGBS) used in this study are shown in Tables 3 and 4, respectively. Polycarboxylate superplasticizer (50% solid content) was used to control the slump and slump flow of fresh concrete, which was above 200 mm and approximately 550 mm, respectively.

Specimens in the forms of 100 mm×100 mm×100 mm cubes and 100 mm×100 mm×300 mm beams were of two types of concrete designated by 0.18UHSC and 0.26HSC. Their mix proportions and compressive strengths are given in Table 5. After casting, all specimens were immediately plastic-wrapped to minimize moisture loss and then stored at room temperature for 24 h. After demolding, all of the specimens were cured in water at 20 °C until 56-day age.

Table 1 Physical properties of coarse aggregate

Type	Apparent density (kg/m ³)	Packing density (kg/m ³)	Crushing index (%)
Basalt	3 030	1 790	3.1

Table 2 Physical properties of artificial sand (fine aggregate)

Fineness modulus	Apparent density(kg/m ³)	Packing density (kg/m ³)	Mud content(%)	Clay pieces content(%)	Stone powder content(%)
2.94	2 600	1 650	5.5	0.5	5.5

Table 3 Cement properties

Cement	Initial setting time(min)	Final setting time(min)	Flexural strength(MPa)		Compressive strength(MPa)	
			3 d	28 d	3 d	28 d
52.5R	137	194	7.4	9.0	37.4	62.0

Table 4 Physical properties of mineral admixtures

Mineral materials	Density(kg/m ³)	Blaine specific surface (m ² /kg)	Loss on ignition (%)
SF	2 200	22 205	1.73
FA	2 520	1 390	1.98
GGBS	2 900	1 020	0.22

Table 5 Mix proportions of concretes

Type	W/B	Binders(kg/m ³)				Sand(kg/m ³)	Basalt(kg/m ³)	Compressive strength at 56-day age (MPa)
		C	SF	FA	GGBS			
0.18UHSC	0.18	540	90	180	90	620	930	139.8
0.26HSC	0.26	540	90	180	90	620	930	109.5

2.2 Determination of Residual Mechanical Properties of Concrete

Cube specimens of 100 mm size were employed for strength determination, and fracture energy tests

were performed on notched beam specimens of 100 mm×100 mm×300 mm, the notch was pre-cut at the mid-span of each specimen during casting. At 56 days, the specimens were pre-dried at 105 °C in

order to reduce moisture content of concrete to a lower degree, so that the specimens for mechanical property determination would not encounter explosive spalling when exposed to high temperature. The specimens were heated in an electric furnace with a heating rate of 2.0 °C/min, and the target temperature was maintained for 2 h. After the specimens cooled naturally to room temperature, residual compressive strength, residual splitting tensile strength, and residual fracture energy of the specimens were measured. Temperature-time curves in heating of the tests with different target temperatures are given in Fig.1. It is noted that the measured temperature is the furnace temperature.

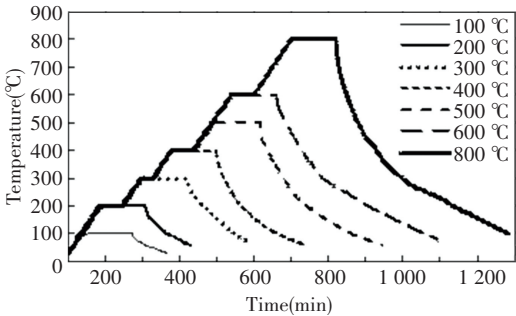


Fig.1 Temperature-time curves in heating of the tests at different target temperatures

The residual compressive strength and tensile splitting strength of the specimens were measured at loading rates of 1.0 and 0.1 MPa/s, respectively. Each result in this study is the average result of three individual results. The fracture energy of the specimens was determined in accordance with RILEM standard-FMC1^[12].

A three-point bending test with displacement-controlled loading rate of 0.05 mm/min was performed on each notched beam specimen. The mid-span deflection δ was recorded during the entire loading process. Upon the load-deflection curve, the fracture energy of the specimens was calculated by using Eq.(1) as specified in the RILEM test method.

$$G_F = \left[\int_0^{\delta_0} P(\delta) + mg\delta_0 \right] / A_{lig} \tag{1}$$

where G_F is the fracture energy (J/m^2), $m = m_1 + m_2$ (kg), $m_1 = Ms/L$ (the weight of the beam support, calculated as beam weight multiplied by s/L), M is the mass of the specimen, m_2 is the weight of the part of the loading arrangement that was not attached to the machine but that follows the beam until failure, s is the span, L is the length of the specimen, $g = 9.81 \text{ m/s}^2$, δ_0 is the mid span deflection of the specimen at failure (m), A_{lig} is the area of the ligament (m^2), δ is the mid-span deflection (m), and P is the load (N).

2.3 Explosive Spalling Test

Explosive spalling tests were conducted on 100 mm cube specimens. Prior to the tests, all of the specimens were dried to designed moisture contents of 0%, 25%, 50%, 63%, 75% or 100%, which were determined by Peng’s method^[13]. Afterwards, the specimens with different moisture contents were heated to 800 °C with a heating rate of approximately 7.5 °C/min in an electric furnace. The air temperature in the electric furnace at a position that 40 mm above the top of the specimens was measured, as shown in Fig.2.

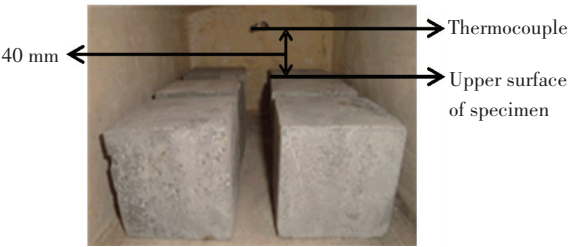


Fig.2 Specimens in the electric furnace before heating

2.4 Microstructure Test

SEM imaging and MIP test were performed to determine the variation in the microstructure of concrete after exposure to the elevated temperatures, and to identify a correlation between the distinct changes in micro-morphology and mechanical properties at macro-scale.

Samples for SEM imaging test were small pieces with thickness of 8 mm. The samples for microstructure analysis in this work were 0.18UHSC specimens after exposure to 20, 100, 200, 400, 600 and 800 °C, and 0.26HSC specimens after exposure to 20, 100, 200, 300 and 400 °C. It is noted that, prior to the tests, the specimens were completely dried and sealed to save testing time.

The pore volume of concrete was measured using MIP. Small particles were taken from the hardened cement paste of specimens after exposure to different high temperatures. The samples were then dried to a constant weight at 105 °C for 48 h in an oven before testing. The samples were subjected to a maximum pressure of up to 413 MPa. A constant contact angle of 130 degree and a constant surface tension of 485 dynes/cm were applied.

3 Results and Discussion

3.1 Residual Compressive Strength

The residual compressive strengths of 0.18UHSC and 0.26HSC after exposure to different target temperatures are plotted in Fig.3. It can be observed that there existed a critical temperature in terms of the effect on the residual compressive strength, which was

400 °C for 0.18UHSC and 300 °C for 0.26HSC. From 100 °C to the critical temperature, the residual compressive strength was increased as the temperature went up, and the peak compressive strength of concrete was observed at the critical temperature. When the temperature was above the critical temperature, the residual compressive strength of concrete began to gradually decrease as the temperature increased and the strength loss tended to be intensified as temperature reached 800 °C.

The peak compressive strengths of 0.18UHSC at 400 °C and 0.26HSC at 300 °C were 32.5% and 2.6% higher than their original strengths at 20 °C, respectively. The increase in compressive strength was attributed to the further hydration of the unhydrated cement and reactive mineral admixtures when exposed to high temperature^[14-15], and the dry hardening at temperatures of 150–350 °C^[16]. While the observed strength loss may be caused by the reduction or disintegration of C–S–H gel and phase transformation from $\text{Ca}(\text{OH})_2$ to CaO ^[17]. 0.18UHSC remained a higher strength growth rate than that of the 0.26HSC due to a denser microstructure of the 0.18UHSC specimens.

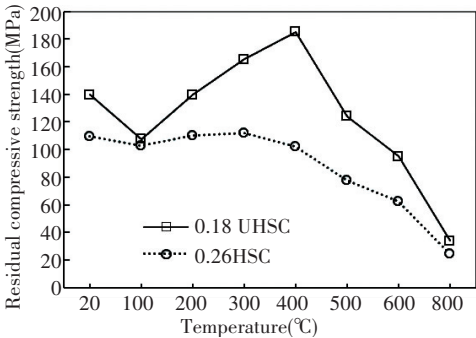


Fig.3 Residual compressive strength of concrete after exposure to various target temperatures

Notably, within the first temperature range, the strength loss at 100 °C is observed in both 0.18UHSC and 0.26HSC, which might be attributed to the internal cracks caused by the escape of free water^[18-19]. Furthermore, the original strength reduction in 0.18UHSC is greater than that in 0.26HSC, which might be explained by a much denser and more brittle microstructure of 0.18UHSC that is more sensitive to cracking.

3.2 Residual Splitting Tensile Strength

The residual splitting tensile strengths of 0.18UHSC and 0.26HSC subjected to different high temperatures are shown in Fig.4. A significant loss in residual splitting tensile strength after exposure to high temperature was observed in both types of specimen and generally, the higher temperature, the higher strength loss rate. After exposure to 800 °C, the

strength losses of 0.18UHSC and 0.26HSC were 79.7% and 82.4% comparing to their original strengths at 20 °C, respectively. The gradual decreasing trend in residual splitting tensile strength noticeably differed from the corresponding changes in the residual compressive strength that discussed above, since the splitting tensile strength is more sensitive to cracks caused by elevated temperature. The present work is in good agreement with Peng’s results^[15].

Change in color was observed on the fracture surface of splitted specimens after exposure to 800 °C, showing dark-gray in the inner region and yellow-beige at the edges. These changes were mainly caused by the decomposition of carbohydrates, followed by the carbon oxidizing after long-term high temperature heating. The color change in the coarse aggregates was extremely pronounced, where the original dark-gray turned into brown. No color change was identified in the specimens after exposure to target temperatures ranging from 20 to 600 °C.

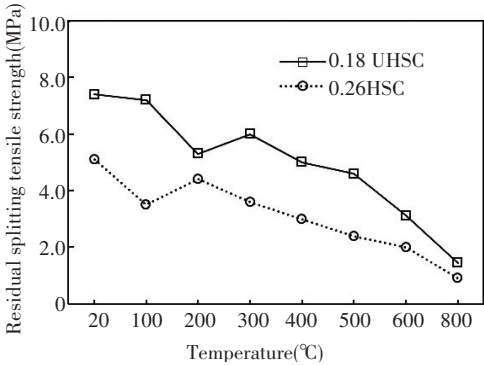


Fig.4 Residual splitting tensile strength of concrete exposed to various target temperatures

The widths of the yellow-beige at the edges are given in Table 6. The yellow-beige region in the 0.18UHSC is thinner than that in the 0.26HSC, suggesting that the damage-resistance of 0.18UHSC is stronger than 0.26HSC after exposure to 800 °C. Petrographic techniques have been used to determine the depth of fire damage to structural concrete by visually inspecting color change^[20]. The width of the dark-gray area varied in different orientations and that at the bottom surface was the smallest, which might be explained by that only the bottom surface of the specimen was tightly close to the internal wall of the furnace, as shown in Fig.2.

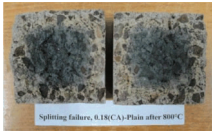
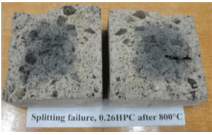
3.3 Residual Fracture Energy

The residual fracture energies of concretes after exposure to different temperatures are shown in Fig.5. The residual fracture energies of both 0.18UHSC and 0.26HSC basically were increased as the temperature increased from 100 to 600 °C. The fracture energy of

concrete reached the maximum value at 600 °C due to the pore structure coarsening induced by high temperature. Another explanation may be that the thermal damage makes the microstructure more heterogeneous and the cracks more tortuous^[21]. Similarly, the residual fracture energy was decreased significantly at 800 °C, but was still slightly higher

than that at 200 °C due to the pore structure coarsening. This can be further evidenced by the load-deflection curves of concrete under loading. For instance, the tails of the load-deflection curves of 0.18UHSC (Fig.6) showed a decreasing slope with increasing temperature from 400 to 600 °C, indicating a large amount of absorbed energy.

Table 6 Widths of the yellow-beige at the edges in the broken surface of concrete exposed to 800 °C after the splitting tensile strength test

Type	Appearance of broken surface	Width of yellow-beige color (mm)		
		Forming surface	Lateral surface	Bottom surface
0.18UHSC		22	22	15
0.26HSC		32	25	20

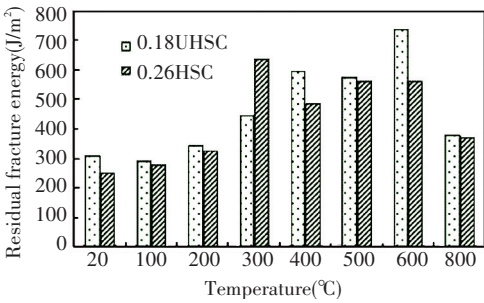


Fig.5 Residual fracture energy of concrete exposed to different target temperatures

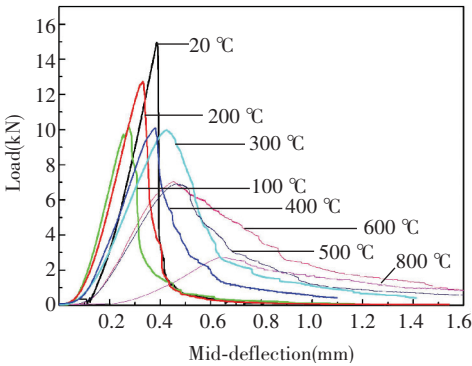


Fig.6 Load-deflection curves of 0.18UHSC subjected to different temperatures during fracture energy testing

3.4 Explosive Spalling

3.4.1 Occurrence of explosive spalling

The statistical results of the occurrence of explosive spalling are detailed in Table 7. Moisture content significantly affected the explosive spalling of

concrete. When the moisture content was below 50%, no spalling was observed in the 0.26HSC specimens, and only one specimen encountered explosive spalling when the moisture content was 63% or 75%. But explosive spalling occurred in the 0.18UHSC specimens with the moisture content of 25%, and all of the 0.18UHSC specimens with the moisture content of $\geq 50\%$ experienced violent explosive spalling. Therefore, at the same moisture content, the explosive spalling of the 0.18UHSC specimens was more serious than that of 0.26HSC. Additionally, the probability and severity of explosive spalling increased with an increased moisture content.

Table 7 Occurrence of explosive spalling in concretes with different moisture contents

Type	Moisture content(%)					
	0	25	50	63	75	100
0.18UHSC	0(3) *	2(6)	6(6)	6(6)	6(6)	6(6)
0.26HSC	0(3)	0(6)	0(6)	1(6)	1(6)	4(6)

* Data inside the parentheses indicates the total number of specimens under each condition, the value outside the parentheses is the number of specimens encountering explosive spalling in this batch.

Appearances of the spalled or damaged specimens (Table 8) indicate that all of the 0.18UHSC specimens spalled into small fragments, suffering considerably severer explosive spalling than the 0.26HSC. This is because the 0.18UHSC has an inherently denser microstructure than 0.26HSC, and the internal vapor pressure, built up due to elevated temperature, is not released quickly from the specimens and thus leads to explosive spalling.

3.4.2 Sieving test

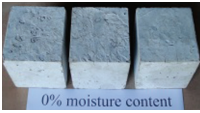





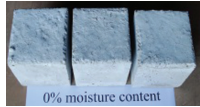

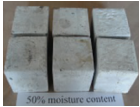
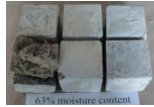
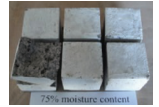

0.18UHSC specimens, particularly those with the moisture contents of above 50% (Fig.7), were sieved to determine the severity of explosive spalling of these specimens at different moisture contents. It can be concluded that moisture content significantly affects the explosive spalling of UHSC, where the higher the moisture content is, the more serious the explosive spalling is. Thus, vapor pressure is a major factor on inducing explosive spalling.

3.5 Relationship between Explosive Spalling and Mechanical Properties

It is commonly accepted that HSC, due to its high brittleness, relatively low permeability and high

compressive strength, is more likely to experience explosive spalling than normal-strength concrete due to the high pore pressure that built up in the dense microstructure of HSC. In this study, the residual compressive strength, residual splitting tensile strength, and residual fracture energy of UHSC were consistently higher than those of HSC while UHSC is more prone to explosive spalling than HSC, and the severity of explosive spalling of the UHSC specimens was higher due to the higher compressive strength of UHSC. These suggest that the occurrence of explosive spalling is closely related to the compressive strength of concrete, the higher the compressive strength is, the higher the probability and severity of explosive spalling are.

Table 8 Appearances of specimens exposed to 800 °C

Type	Moisture contents(%)					
	0	25	50	63	75	100
0.18UHSC						
0.26HSC						

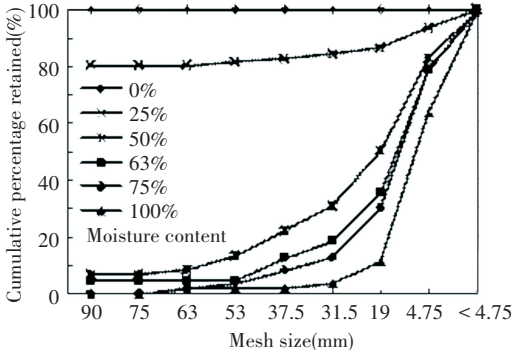


Fig.7 Particle size distribution of the 0.18UHSC specimens with different moisture contents after explosive spalling test

Explosive spalling is essentially in the form of severe cracking, and the plain UHSC without any fiber has poor crack-resistance behavior thus resulting in the more serious explosive spalling. The splitting tensile strength and fracture energy of concrete have a positive correlation with its resistance to cracking, but the peak splitting tensile strength and fracture energy of the plain UHSC without any fiber were lower than 8.0 MPa and 800 J/m², respectively. Thus, the fact that the tensile strength and fracture energy of UHSC were higher than those of HSC cannot play a role in preventing the great cracking in the UHSC specimens.

Therefore, the explosive spalling of the plain UHSC is more closely related to its compressive

strength than with its other mechanical properties, the higher the compressive strength of concrete is, the severer the explosive spalling is. Steel fiber has an excellent cracking-resistance, its influence in the mechanical properties and the occurrence of explosive spalling of UHSC needs to be further studied.

In engineering structures, explosive spalling may result in the loss in load-bearing capacity due to the damage of structural elements in fire, such as the reduction of cross-sectional area and the loss of the protection that concrete cover provides to steel reinforcement. The reinforcement without the protection of concrete cover can readily reach an extreme temperature, which results in the reduction in yielding strength of rebar. Thereby, the damage in structural elements by explosive spalling may trigger an integrity failure of reinforced concrete structure.

3.6 Microstructure Analysis

3.6.1 SEM observation

SEM observation can identify a correlation between the changes in microstructure and compressive strength of concrete. The SEM images of both 0.18UHSC and 0.26HSC specimens after exposure to different temperatures are given in Figs. 8 and 9, respectively. The microstructures of both 0.18UHSC and 0.26HSC were relatively dense at 20 °C, and calcium silicate hydrate (C-S-H) gel was in the form of continuous block. After exposure to 200 °C, the C-S-H

gel filled the micro pores and a denser internal structure formed in the 0.18UHSC specimens while the features were not obvious in the 0.26HSC specimen. At 400 °C, the C-S-H gel in 0.18UHSC continued to grow, and yielded the densest microstructure, resulting in the highest compressive strength of concrete. But cracks were clearly observed in the 0.26HSC specimen, which led to the degraded compressive

strength compared with that at 300 °C. At 600 °C, the complete C-S-H gel bulk degenerated into wollastonite. Meanwhile, the pore structure coarsening was increasingly serious. These resulted in a significant decrease of compressive strength of concrete. After heating to 800 °C, wollastonite degenerated partially, and a large number of pores were observed. The results are consistent with previous works^[22-23].

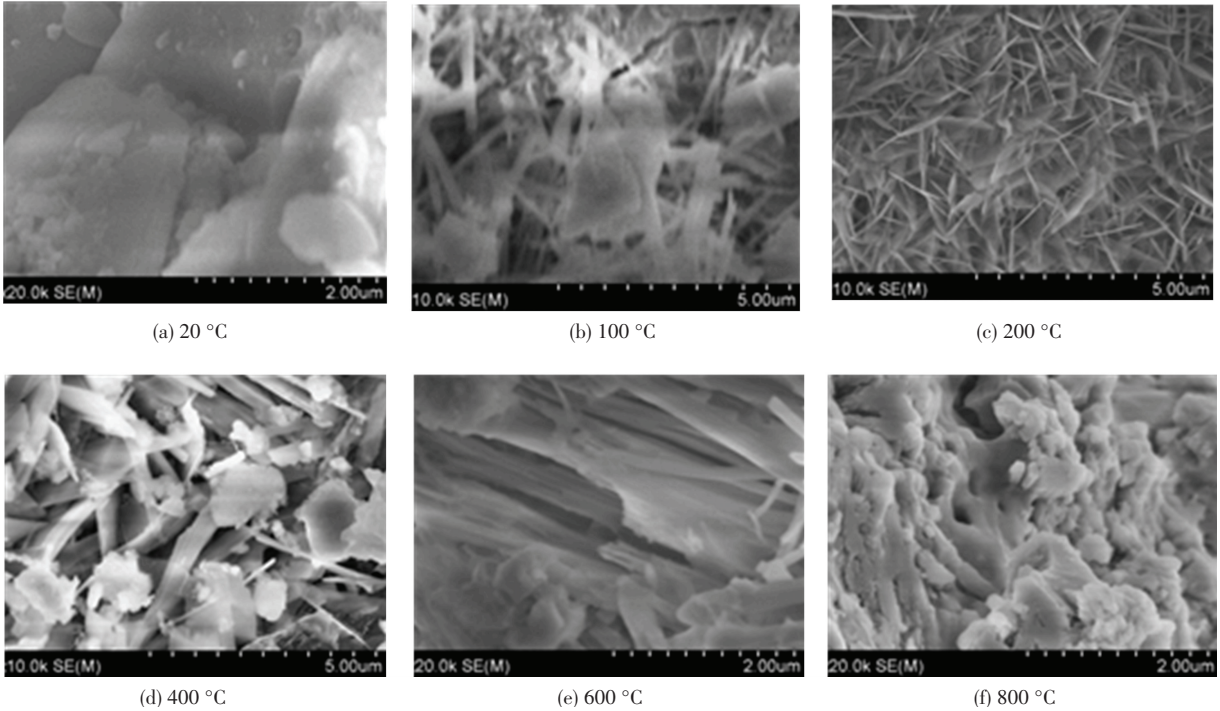


Fig.8 SEM images of the 0.18UHSC specimens after exposure to different high temperatures

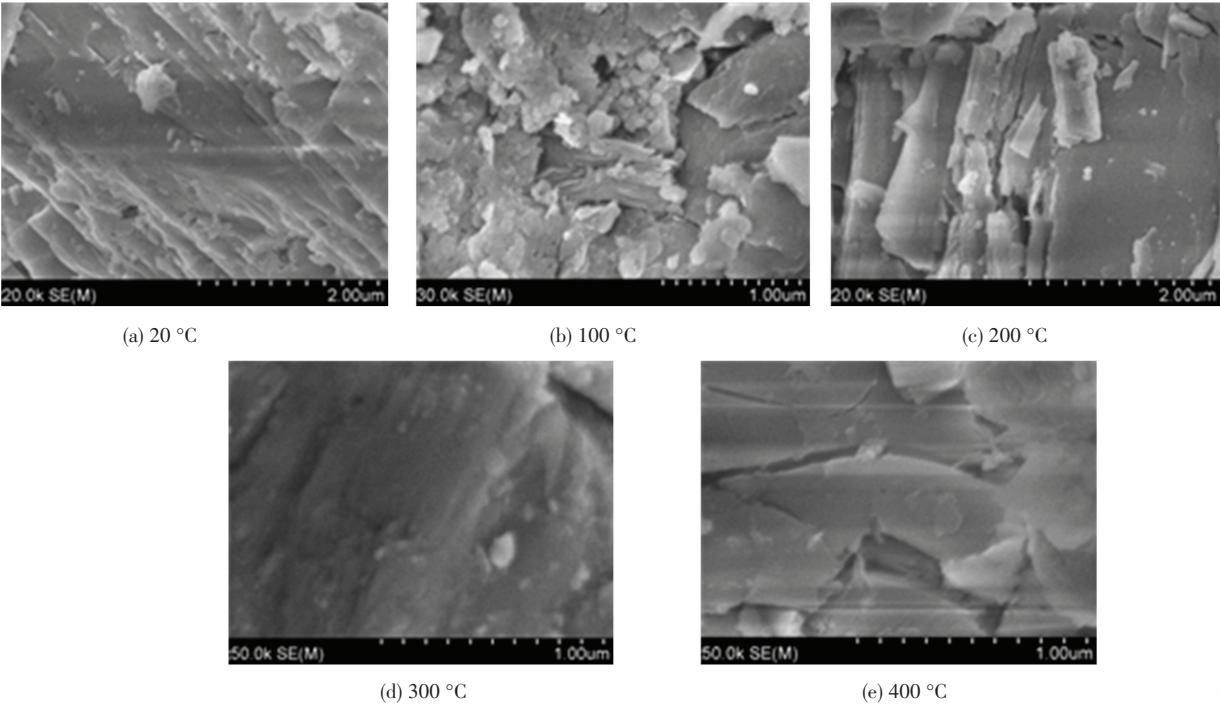


Fig.9 SEM images of the 0.26UHSC specimens after exposure to different high temperatures

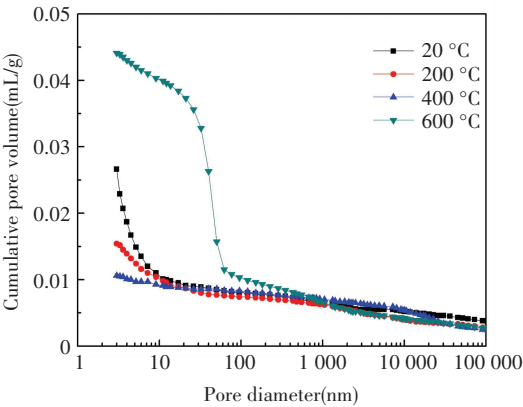
In addition, the energy spectrum analysis of the hydration productions in the SEM images may further verify the different crystal formations in the microstructure of concrete, which definitely affect compressive strength of concrete. At 200 °C, C-S-H gels have transformed into tobermorite ($\text{Ca}_5\text{Si}_6\text{O}_{16}(\text{OH}) \cdot 5\text{H}_2\text{O}$ or $\text{C}_5\text{S}_6\text{H}_5$) with a Ca/Si ratio of 0.83, which is denser than C-S-H gels. At 250 °C, the xonotlite crystal was formed with a Ca/Si ratio of 1.0 and had a better rigid structure^[24]. After exposure to 400 °C, plenty of crystals with a Ca/Si ratio of 1.0 were found in the microstructure of concrete, which was xonotlite. Thus, below 400 °C, compressive strength of UHSC was significantly increased with the temperature increasing.

It is noted that, after exposure to 100 °C, cracking is observed in the 0.18UHSC specimens, which results in a significant decrease of compressive strength of concrete while the cracking in cement paste in 0.26HSC is considerably less pronounced. Chi-Ming Tam^[24] also identified the cracks in the reactive power concrete samples at 100 °C with an exposure time for 8 h. However, the exposure time at 100 °C in this study is less than 3 h. Whether the cracks are resulted from the escape of free water or not, this needs to be further researched.

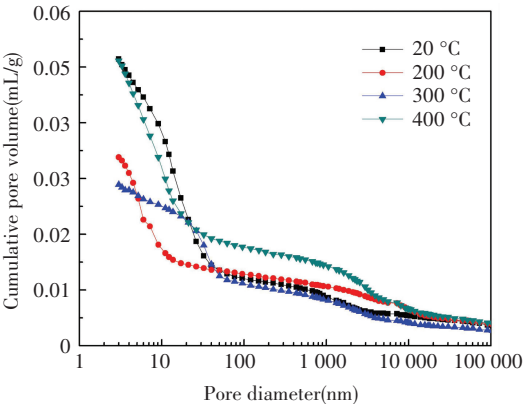
3.6.2 Pore structure

Pore structure is essential to understand the explosive spalling behavior of concrete exposed to high temperature. Fig.10 shows the cumulative pore volume of the 0.18UHSC and 0.26HSC specimens after exposure to different temperatures. After exposure to high temperatures ranging from 20 to 400 °C, the cumulative pore volume of the 0.18UHSC specimen gradually decreased, and concrete had a much denser structure. But the C-S-H gel in the 0.26HSC specimen cracked at 400 °C, and the pore structure coarsening was serious, which resulted in a significant increase of pore volume compared to that at 300 °C. This can explain that the peak compressive strength of the 0.26HSC was obtained at 300 °C, and the temperature range, in which the cumulative pore volume continued to reduce, is from 20 to 300 °C.

Moreover, after exposure to the same temperature, the cumulative pore volume of the 0.26HSC specimen is much higher than that in the 0.18UHSC specimen. It can be concluded that UHSC which is denser than HSC has a lower permeability and porosity due to its lower W/B. This resulted in that less vapor could escape, and higher vapor pressure was built up. Subsequently, enough pore pressure induced explosive spalling. Thus, pore structure significantly affects the explosive spalling, and the severity of explosive spalling of UHSC is much higher than that of HSC.



(a) 0.18UHSC



(b) 0.26HSC

Fig.10 Pore volume of the 0.18UHSC and 0.26HSC specimens

4 Conclusions

1) As the temperature increased, the residual compressive strengths of UHSC and HSC were first increased and then decreased. The increment of residual compressive strength of the UHSC at the critical temperature of 400 °C, at which the peak compressive strength was obtained, was much higher than that of the HSC. The residual splitting tensile strengths of both types of concrete continued to decrease. After exposure to 800 °C, the loss in compressive strength or splitting tensile strength exceeded 70%. The residual fracture energies of both concretes tended to ascend even at 600 °C, and then were decreased significantly at 800 °C.

2) Moisture content significantly affected the explosive spalling of both UHSC and HSC, and the higher the moisture content is, the more serious the explosive spalling is. There was a positive correlation between moisture content and the severity of explosive spalling, and it is more pronounced in UHSC. When the moisture content was not lower than 50%, all of the UHSC specimens spalled into many fragments while only a few of the HSC specimens spalled. This suggests

that the probability and the severity of explosive spalling of the UHSC specimens are much higher compared with HSC, and vapor pressure is the main factor on inducing explosive spalling.

3) A correlation existed between the changes in the microstructure of both UHSC and HSC specimens and the residual compressive strength of concrete after exposure to different temperatures. Below the critical temperature, C-S-H gel gradually increased in various forms, reduced the porosity and enhanced the inner structure, thus improving the compressive strength of concrete. Above the critical temperature, the decomposition of C-S-H gel and pore structure coarsening were contributed to the strength loss.

4) Pore structure significantly affected the explosive spalling, the lower the porosity of concrete is, the more serious the explosive spalling is. Thus, the severity of explosive spalling of UHSC was much higher than that of HSC due to the denser microstructure of UHSC.

References

- [1] Kojima M, Mitsui K, Wachi M. Application of 150 N/mm² advanced performance composites to high-rise R/C building. Proceedings of 8th International Symposium on Utilization of High-Strength and High-Performance Concrete. Japan, 2008. 1199–1206.
- [2] Riedel W, Markus N, Elmar S. Local damage to ultra-high performance concrete structures caused by an impact of aircraft engine missiles. Nuclear Engineering and Design, 2010, 240: 2633–2642.
- [3] Lu L J. Construction technology of C100 high performance concrete in National Great Theater. Construction Technology, 2003, 32(9): 48–50. (in Chinese)
- [4] Gu G R. Preparation, production and ultra-high pumping technology of C100 self-compacting concrete and C100 in Xita building. China Concrete, 2009, 7(1): 31–41. (in Chinese)
- [5] Dong Y N, Su L N, Xiao L Q. Concrete construction technology of Shenyang Huangchao Wanxin building. Coal Technology, 2011, 9: 140–141. (in Chinese)
- [6] Sakuragi F, Suzuki K, Kanda T. Development research on fire-resistance of ultra-high strength concrete (five small-sized samples). Proceedings of Academic Lecture of the Japanese Society of Architecture. 1992. 479–480.
- [7] Keiichi M, Tomio O, Sakuragi F. The development research on fire-resistance of ultra-high strength concrete (six actual full-sized RC cylinders). Proceedings of Academic Lecture of the Japanese Society of Architecture. 1992. 481–482.
- [8] Hosser D, Kampmaier B, Hollmann D. Behavior of ultra-high performance concrete (UHPC) in case of fire. Proceedings of HiperMat (3rd International Symposium on UHPC and Nanotechnology Symposium on UHPC Construction Materials). Kassel, Germany, 2012. 573–582.
- [9] Lin L X, Ye H A, Feng N Q. Experimental research on improving the brittleness of C120 concrete with ultra-high strength by adding polypropylene fiber. Industrial Construction, 2012, 42(11): 1–5. (in Chinese)
- [10] Masuda T, Koji T, Yamada H. Research on fire-resistance of ultra-high strength reinforced concrete cylinder (eleven concrete cylinders, $F_c = 150 \text{ N/mm}^2$). Proceedings of Academic Lecture of the Japanese Society of Architecture. 2005. 79–80, 9.
- [11] Mitsui K, Yonezawa T, Kojima M. Fire-resistance of ultra-high strength concrete cylinder with the design strength of 80~200 N/mm² and the influence of organic fiber on it). Proceedings of Academic Lecture of the Japanese Society of Architecture, 2010, 75(648): 461–468.
- [12] RILEM. FMC1 Determination of the fracture energy of mortar and concrete by means of three-point bend tests on notched beams. RILEM Technical Recommendations for the Testing and Use of Construction Materials, E and FN SPON. London, 1994. 99–101.
- [13] Peng G F, Chen Y N, Anson M. Explosive spalling thermally induced and fire property of high performance silica fume concrete. Journal of Building Materials, 1999, 2(3): 193–198.
- [14] Chen Y N, Peng G F, Anson M. Residual strength and pore structure of high-strength concrete and normal strength concrete after exposure to high temperatures. Cement and Concrete Composites, 1999, 21(1): 23–27.
- [15] Peng G F, Kang Y R, Huang Y Z. Experimental research on fire resistance of reactive powder concrete. Advances in Materials Science and Engineering, 2012(7). DOI: 10.1155/2012/860303.
- [16] Phan L T. Fire performance of high-strength concrete: A report of the state-of-the-art. Gaithersburg: Rep. NISTIR 5934, p. 105. National Institute of Standards and Technology, 1996.
- [17] Peng G F, Huang Z S. Change in microstructure of hardened cement paste subjected to elevated temperatures. Construction & Building Materials, 2008, 22(4): 593–599.
- [18] Schneider U, Diederichs U, Horvath J. Verhalten von ultrahochfesten betonen (UHPC) unter brandbeanspruchung. Beton-und Stahlbetonbau, 2003, 98(7): 408–417.
- [19] Zheng W Z, Luo B F, Wang Y. Compressive and tensile properties of reactive powder concrete with steel fibers at elevated temperature. Construction and Building Materials, 2013, 41: 844–851.
- [20] Ingham J P. Application of petrographic examination techniques to the assessment of fire-damaged concrete and masonry structures. Materials Characterization, 2009, 60: 700–709.
- [21] Bamonte P, Gambarova P G. Properties of concrete subjected to extreme thermal conditions. Journal of Structural Fire Engineering, 2014, 5(1): 47–62.
- [22] Tai Y S, Pan H H, Kung Y N. Mechanical properties of steel fiber reinforced reactive powder concrete following exposure to high temperature reaching 800 °C. Nuclear Engineering & Design, 2011, 241(7): 2416–2424.
- [23] Zheng W Z, Li H, Wang Y. Compressive behaviour of hybrid fiber-reinforced reactive powder concrete after high temperature. Materials & Design, 2012, 41: 403–409.
- [24] Tam C M, Wing V, Yan T. Microstructural behaviour of reactive powder concrete under different heating regimes. Magazine of Concrete Research, 2012, 64(3): 259–267.